Experimental study of crack identification in thick beams with a cracked beam element model

Experimental study of crack identification in thick beams with a cracked beam element model

Chuanchuan HOU [1] and Yong LU, F.ASCE [2]

[1] Ph.D. Student, Institute for Infrastructure and Environment, School of Engineering, the University of Edinburgh, Edinburgh EH9 3JL, UK.

[2] Professor, Institute for Infrastructure and Environment, School of Engineering, the University of Edinburgh, Edinburgh EH9 3JL, UK (corresponding author). E-mail: yong.lu@ed.ac.uk

Abstract

Model-based crack identification in beam-like structures has been a classic problem. The authors have recently developed a framework to identify crack damage in beams based on a cracked beam element model, which stems from the local flexibility and fracture mechanics principles. This paper presents an experimental study on the cracked beam element model for crack damage identification in a physical testing environment. Five solid beam specimens were prepared with different numbers of cracks, and they were subjected to a modal testing and analysis procedure to extract the natural frequencies and mode shapes. The extracted modal data were then compared with the predicted counterparts using the cracked beam element model to verify the accuracy of the model. The extracted modal data were also employed to inversely identify the cracks with the cracked beam element model through a model updating procedure. Results indicate that all the cracks can be identified correctly with accurate crack depth and location information. To enhance the modal dataset for FE model updating, the so-called 'artificial boundary condition' (ABC) technique has also been applied on the test beams, and the incorporation of such frequencies proves to enhance the identification of cracks from the FE model updating.

Keywords: Cracked beam element model, beam experiment, modal testing, rational fraction polynomial, crack identification, artificial boundary condition

Introduction

The crack identification of beam-like structures based on vibration response is a classic problem and has been extensively studied in the past. Generally, the various identification methods can be subdivided into model-based and non-model-based methods. In the model-based methods which are of particular interest in the present study, an appropriate computational model for the structure, be it a detailed finite element (FE) model or a simplified structural model, is required to represent the dynamic properties of the physical structure. The variable parameters (properties) of the model can then be updated by matching the computed modal data from the model with the extracted modal data from the actual structure. The damage states are identified by examining the respective updated properties as damage indicators. Typically a combination of frequency and mode shape data may be employed in such a procedure; however a number of studies have concentrated on crack identification in beams with frequency-only information, both for single-crack (e.g. Narkis, 1994; Lee and Chung, 2000; Morassi, 2001; Swamidas et al., 2004; and Rubio et al., 2015a) and multiple-crack (e.g. Ruotolo and Surace, 1997; Sinha et al., 2002; and Rubio, et al. 2015b) scenarios.

In a model-based damage identification approach, it is essential that the model being used is capable of representing the actual structure, particularly in terms of the effect of the damage, in a robust manner so as to reduce the basic model errors. One typical source of such model errors arises from the modelling of cracks, the behaviour of which can be quite complicated in the vibration of beam-like structures.

There has been a lot of research effort in attempt to develop simple and reliable crack models in the past. Some of the crack models have been summarized in Friswell and Penny (2002). The authors of the present paper have also carried out a comprehensive review and comparison of existing beam crack models concerning their effectiveness in describing the

vibration properties (Hou, C. C., and Lu, Y., "Identification of cracks in thick beams with a cracked beam element model," submitted, the University of Edinburgh, Edinburgh, UK). Generally the models may be subdivided into four categories, namely a) reduced stiffness model, b) models based on stress fields, c) models based on a discrete spring scheme, and d) models based on local flexibility and fracture mechanics. Demonstrative analyses on relatively thick cracked beams (beams with a length to sectional depth ratio in the range of 5 to 15) show that the reduced stiffness model has an inherent inconsistency problem, in that for the same cracked scenario different stiffness reductions will result if the modal data such as natural frequencies from different modes are to be represented. In other words, the effect of a given actual crack will manifest as different stiffness reductions with respect to different modes. Models based on stress fields and models based on discrete springs can better deal with the above issue, but generally speaking the cracked beam element model formulated on the basis of additional flexibility and fracture mechanics is deemed to provide the best representation of a crack concerning practically all modes of interests.

Such a cracked beam element model as adopted in the present study has its element stiffness matrix formulated with explicit parameters relating to the location of a crack within the element and its severity (depth). The model also takes into account specific aspects concerning the vibration properties of thick beams, including shear deformation and rotational inertia as well as the coupling between flexural and axial modes. In a numerical simulation study, in which the “real” effect of the crack on the dynamic properties of the beam was simulated by refined solid finite element model allowing explicit representation of the cracks, and then compared with the predictions using the cracked beam element in a Timoshenko beam model, the cracked beam element model proved to perform well even for relatively high modes. The natural frequencies and mode shapes up to the 9^{th} mode have been predicted with satisfactory accuracy using the cracked beam element. When implemented in

77 an inverse procedure, very good crack identification results, both for a single crack and for
78 multiple-crack scenarios, have been achieved with numerically simulated modal data from
79 the refined finite element model.

80 While the theoretical concepts and principles underlying the development of the cracked
81 beam element model may reasonably be examined against results generated from the
82 aforementioned finite element simulations, physical experiments are still indispensable in
83 order to test the behaviour of the theoretical model in a real measurement environment.
84 Experimental studies serve also to further verify the accuracy of the crack beam element and
85 its effectiveness in crack identification given the various constraints that exist in an
86 experimental condition.

87 There have already been many experimental modal testing studies relating to the effects
88 of cracks on the beam vibration properties and the development of crack models. Christides
89 and Barr (1984) extracted the lowest few natural frequencies of simply-supported intact and
90 cracked steel beams to calibrate the stress decay rate assumed in the crack model. Chondros,
91 et al. (1998) tested simply-supported intact and cracked aluminium beams to verify a crack
92 model developed based on the stress distribution around the crack location; however only the
93 fundamental natural frequency was extracted and used in the verification. Swamidas, et al.
94 (2004) conducted modal testing on a slender aluminium beam with a varying crack depth
95 ratio from 0.1-0.5. The first four natural frequencies were obtained and used to verify the
96 developed vibration theory for cracked Euler's beam. Ruotolo and Surace (1997) tested
97 beams with multiple cracks. Three slender cantilever steel beams, each had two cracks, were
98 tested and the first 4 natural frequencies and mode shapes were obtained. Crack identification
99 was then conducted on the beams through model updating. Sinha, et al. (2002) conducted
100 experimental modal testing and employed the test results to verify a cracked beam element,
101 which was developed based on Euler-Bernoulli beam element with modified local flexural

rigidity distribution in the vicinity of cracks.

It should be pointed out that most of the existing experiments have been conducted on rather slender beams. However, the relative effect of different methods with which a crack is modelled tends to diminish as the beam slenderness increases. According to a comparative study by Friswell and Penny (2002), several types of crack models, namely the simple reduced stiffness model, the discrete spring model, the model by Sinha, et al. (2002), and the model presented in Lee and Chung (2000) based on fracture mechanics, could predict the first 3-5 mode natural frequencies of cracked slender beams with similar accuracy. For a more stringent verification of a beam crack model it would be appropriate to employ sufficiently 'thick' beams, which are also more representative of beam members in civil engineering applications where a length to depth ratio is typically in the region of 10-15. Furthermore, some of the important effects of a crack, such as the local shear deformation and the coupling of different vibration modes, can only be observed properly from the vibration of thicker beams.

This paper presents an experimental study on the effectiveness of the cracked beam element model for identification of cracks in relatively thick beams. To test the robustness of the theoretical model, thick beam specimens with a single crack or multiple cracks at arbitrarily selected locations have been prepared. Modal tests have been carried out on these beams to extract the first few natural frequencies and mode shapes. The extracted modal data are compared with the predicted results using the cracked beam element model. On the other hand, the extracted modal data are also employed in an inverse crack identification procedure by means of finite element model updating, and the identified crack parameters (location and crack depth) are checked against the actual cracks in the beams. Furthermore, extended modal frequencies based on the concept of 'artificial boundary condition' frequencies have been extracted from the experiment as well. These frequencies, herein referred to as "ABC"

127 frequencies and will be discussed in some more detail later, are the equivalence of the
128 conventional perturbed boundary method and may be looked upon as an extension of the
129 transmission zeros of driving frequency response function (FRF) curves. The incorporation of
130 these frequencies helps reduce the reliance on the mode shape data and it proves to be
131 effective for the identification of the crack parameters with the cracked beam element model.

132 **Overview of the cracked-beam element model and numerical verification**

133 The cracked beam element model adopted in this study for crack damage identification
134 incorporates the effect of a crack directly into the element stiffness matrix. The formulation
135 of the cracked element stiffness matrix stems from the consideration of an additional local
136 flexibility, which is derived from fracture mechanics principles. In this way, the cracked
137 beam element model (cracked stiffness matrix) carries explicit parameters defining the crack
138 location within the element as well as its severity (crack depth). The model also considers the
139 shear deformation and the coupling between the longitudinal and transverse deformations.
140 Detailed information of the model can be found in (Hou, C. C., and Lu, Y., "Identification of
141 cracks in thick beams with a cracked beam element model," submitted, the University of
142 Edinburgh, Edinburgh, UK). A brief overview of the model is given below.

143 The concept of local flexibility matrix of the cracked beam element was introduced in the
144 1980's (Dimarogonas and Papadopoulos, 1983; Papadopoulos and Dimarogonas, 1987a;
145 1987b), and it is based on the relationship between the energy release rate G for a crack
146 growth and the increment of total strain energy U_T due to the crack, as shown in Eq. (1).

147 $$U_T = U_0 + U_c \tag{1a}$$

148 $$U_c = \int_{A_c} G \mathrm{d}A \tag{1b}$$

149 where U_0 is the strain energy of the intact structure under the constant load with shear strain
150 energy counted, and it can be calculated by:

$$U_0 = \frac{1}{2}\int_0^{l_e}\left[\frac{(M + Ql_e - Qx)^2}{EI} + \frac{Q^2}{GA_e} + \frac{P^2}{EA}\right]dx \tag{2}$$

where A_e is the effective shear area of the beam section.

U_c is the additional strain energy brought by the crack, and A_c is the effective crack area. The energy release rate G can be calculated with the Stress Intensity Factors (SIFs) of the crack (Tada, et al., 2000), as:

$$G = \frac{1}{E'}\left(K_I^2 + K_{II}^2 + \frac{1}{1-\nu}K_{III}^2\right) \tag{3}$$

where, K_I, K_{II}, and K_{III} are the stress intensity factors for three different types of cracks, namely opening, sliding and tearing. For plane stress, $E'=E$, and for plane strain, $E'=E/(1-\nu)$, where ν is the Poisson's ratio of the material.

For a cracked beam element with the full 6 degrees of freedom (DOFs) in the two dimensional space shown in Fig. 1 (with crack location l_c within the element and crack depth a), the flexibility of the cracked element can be calculated using Castigliano's theorem, as:

$$c_{ij} = \frac{\partial^2 U_T}{\partial F_i \partial F_j} = \frac{\partial^2 U_0}{\partial F_i \partial F_j} + \frac{\partial^2 U_c}{\partial F_i \partial F_j} \tag{4a}$$

or

$$c_{ij} = c_{ij,0} + c_{ij,c} \tag{4b}$$

where, c_{ij} is the total local flexibility and F_i is the force applied on the i^{th} DOF of the beam node ($F_1=P$, $F_2=Q$, $F_3=M$). $c_{ij,0}$ is the flexibility of the intact beam element, and $c_{ij,c}$ is the additional flexibility due to the presence of the crack.

With Eq. (1) to (4), the local flexibility matrix **C** can be calculated as:

$$\mathbf{C} = \begin{bmatrix} \frac{l_e}{EA} + c_{11,c} & c_{12,c} & c_{13,c} \\ c_{21,c} & \frac{l_e}{GA_e} + \frac{l_e^3}{3EI} + c_{22,c} & \frac{l_e^2}{2EI} + c_{23,c} \\ c_{31,c} & \frac{l_e^2}{2EI} + c_{32,c} & \frac{l_e}{EI} + c_{33,c} \end{bmatrix} \tag{5}$$

In the matrix, the terms $c_{ij,c}$ can be calculated as:

$$c_{ij,c} = \frac{\partial^2}{\partial F_i \partial F_j} \int_0^a \frac{b}{E'} \left[\left(\frac{P}{bh} \sqrt{\pi a} F_{\mathrm{I}1}(\alpha) + \frac{6(M + Ql_e - Ql_c)}{bh^2} \sqrt{\pi a} F_{\mathrm{I}2}(\alpha) \right)^2 + \left(\frac{Q}{bh} \sqrt{\pi a} F_{\mathrm{II}}(\alpha) \right)^2 \right] \mathrm{d}a \quad (6)$$

where, $F_{\mathrm{I}1}$, $F_{\mathrm{I}2}$, F_{II} are dimensionless terms in the SIFs shown in Eq. (3), which can be found in Tada, et al. (2000).

With the local flexibility matrix, the complete 6×6 stiffness matrix for the cracked beam element can be obtained by inverting the flexibility matrix, and it can be written as:

$$\mathbf{K_c} = \mathbf{T}\mathbf{C}^{-1}\mathbf{T}^{\mathrm{T}} \quad (7)$$

where **T** is a 6×3 transformation matrix, and can be expressed as,

$$\mathbf{T} = \begin{bmatrix} -1 & 0 & 0 & 1 & 0 & 0 \\ 0 & -1 & -l_e & 0 & 1 & 0 \\ 0 & 0 & -1 & 0 & 0 & 1 \end{bmatrix}^T \quad (8)$$

In the present study, the cracked element stiffness matrix considering the above crack-induced additional flexibility has been formed on the basis of a Timoshenko beam element with axial force effect. The cracked beam element model in representing the effect of a crack on the vibration properties of relatively thick beams has been verified using simulated modal data generated from 'numerical experiment' with a refined finite element continuum model as explained in the 'Introduction' section. A typical comparison between the predicted natural frequencies using the present cracked beam element model and the simulated data from the refined FE model is shown in Fig. 2. The example beam has a cross section as 100 × 100 mm. and the elastic modulus is set as 210 GPa. Note that to focus on the relative effect of the cracks the comparison is made in terms of the relative frequency change (shift) of the cracked beam from the respective intact state.

Shown in the figure is also a prediction using the traditional "reduced element stiffness" approach for a comparison. This method assumes an equivalent reduced elemental stiffness to

represent the effect of a crack, which effectively leads to a proportionally reduced element stiffness matrix as:

$$\mathbf{K}_{\mathrm{d}} = (1 - D)\mathbf{K}_0 \tag{9}$$

where, $\mathbf{K}_0$ and $\mathbf{K}_{\mathrm{d}}$ are the stiffness matrix of the intact and damaged beam element, respectively. More details about the application of this method for the cracked beam will be provided in the "Verification" section later.

It can be seen that the present Timoshenko-cracked beam element model can predict the natural frequencies of the actual (FE simulated) cracked beam with very good accuracy and the accuracy is consistent for all the first 6 modes. On the contrary, the prediction using the reduced stiffness model could only match some of modes while considerable errors occur for the other modes.

Experimental programme

An experimental programme of modal testing has been conducted with a focus on the effect of cracks on thick beams, for which the cracked beam element model is expected to be particularly effective, and thereby verify the accuracy of the cracked beam element model. To cover different possible crack damage scenarios, different combinations of the cracks, including single-crack and multiple-crack scenarios and with different crack depths, were represented in the test beam specimens.

Test specimens

Five beam specimens were prepared for the tests. The beams were prepared in reduced scale and were made of aluminium. The choices of the material and the sizes have been made mainly for the sake of easy handling especially the creation of the cracks (by saw cuts), and they should not affect the comparative results. All beams had the same overall dimension of $L \times b \times h$ = 600 × 50.8 × 50.8 mm, with L, b and h being the span length, and width and height

of the solid cross-section, respectively. The length to sectional thickness (depth) ratio of the beams is thus about 12, which is representative of the category of thick beams.

The crack conditions of the test beams are shown in Fig. 3, with labels of the beams as B0, B1-B4 in sequential order. Beam B0 was an intact beam as the reference. B1 and B2 both contained a single crack at the same location, but the cracks had different depths. B3 and B4 both had multiple (3 here) cracks of different depths; but B3 had more distinctly spaced cracks, whereas B4 had two of the cracks closely spaced to each other. Therefore, the specimens covered comprehensively the various aspects of cracked beams that may be of practical interest. All the cracks were created using saw cuts, and the width of each cut was approximately 1 mm. Using thin notches to represent cracks is a common practice in laboratory studies and it is worth noting that the stress intensity factors for crack tips are fully applicable to the tips of deep slender notches (Swamidas, et al., 2004; Caddemi and Morassi, 2013; Tada, et al., 2000). It has also been shown that the same local flexibility models arising from Linear Fracture arguments can be used to describe the macroscopic effect of a notch in a beam (Cabib, et al., 2001; Caddemi and Morassi, 2013).

Detailed information of the cracks (thin notches) is shown in Table 1, in which α represents the crack to sectional depth ratio, and L_c is the distance between the crack location and the left end of the beam.

Modal testing setup

The tested beam was suspended with two strings at the two ends to create a free-free boundary condition, as shown in Fig. 4. Hammer impact was used to apply excitation on the beam using a precision impact hammer (B&K type 8206-002) with an aluminium head. Trial tests indicated that with the aluminium head on the hammer a relatively flat impact force spectrum in the range of 0-10000 Hz could be achieved, and this well covered the frequencies of interest for the first several modes. The acceleration response of the beam was measured

241 by light-weight accelerometers (B&Kjær Delta Tron® 4508 type), which have a measurement
242 range of ±700 m/s^2. The mass of the accelerometers is about 5 grams and is negligible with
243 respect to the mass of the test beam over a small segment length.

244 The impact force and acceleration data were recorded with a data acquisition system (NI-
245 9234). The sampling rates for both the impact force and acceleration were set to be 25600 Hz,
246 which was dictated by the need of capturing the detail of the impact force. The record
247 duration of the signals were set to be 16 s. It was found that the record time was just long
248 enough to allow the vibrations to die out, thus eliminating the leakage problem in the
249 subsequent modal analysis.

250 Both the natural frequencies and mode shapes of the beams were extracted from the
251 modal testing. To extract the mode shapes, 11 uniformly distributed measurement locations
252 were marked on the beam, as shown in Fig. 4. During the tests, two accelerometers were
253 attached at point P4 and P10 while impact was applied at each measurement location from P1
254 to P11 in a routine procedure. The amplitudes of the mode shapes at these 11 measurement
255 locations were extracted from the frequency response function (FRF) curves and will be
256 referred as 'mode shapes' in the following descriptions.

257 The FRF curves were calculated from the Fourier transform of the acceleration and
258 impact force signals. As the actual excitation input by the hammer impact lasted only for a
259 very short duration, generally less than 1ms, a force window was employed to eliminate the
260 apparent noises in the remaining much longer recording period. 10 repeated tests were
261 performed for each excitation location and the FRF curves from the repeated tests were
262 averaged for the subsequent use in the extraction of the modal frequencies and mode shapes.

263 ***Modal testing results***

264 Representative FRF curve of beam B0 is presented in Fig. 5. It shows very clear
265 resonances as well as anti-resonances. The natural frequencies and mode shapes of the beams

266 can be extracted from the FRF curves easily using the standard peak-picking method. The
267 lowest five modes of natural frequencies (f_N) are shown in Table 2. It can be seen that the
268 frequency shifts brought by the cracks are generally in the range of 1%-15%, and can be as
269 large as 20% for some specific modes and damage scenarios. The mode shapes can be
270 obtained from the amplitudes of the resonances in the FRF curves. The first two
271 displacement-normalized mode shapes for all specimens are presented in Fig. 6. At this
272 juncture it should be noted that the arrangement of the relatively coarse measurement grid
273 was not aimed to obtain very smooth mode shape curves; instead it was aimed to restrict the
274 number of mode shape data points to represent a practical measurement scenario.
275 Nevertheless the accuracy of the mode shape data at the measured points is not affected by
276 the mode shape resolution.

277 **Verification of the prediction of modal properties by the cracked beam element model**

278 The cracked beam element model outlined in the 'Overview of the cracked beam element
279 model and numerical verification' is verified against the extracted modal testing results in
280 this section. The intact and cracked beams are modelled with Timoshenko beam elements
281 with high-accuracy cubic shape functions. 12 beam elements with uniform element length of
282 50 mm are used in the numerical models. This makes each element in the numerical model to
283 have a length comparable to the actual beam depth, and this is regarded as appropriate
284 considering that the crack influence range is generally about the order of the beam depth. For
285 the same reason, further refinement of the mesh is deemed unnecessary with the use of the
286 present cracked beam element model. Define the distance of the crack to the left end of the
287 respective cracked element as l_c. With the above chosen numerical model setting, the crack
288 will be in the 8th element for beam B1 and B2 (l_c = 25 mm), in the 3rd, 5th and 9th elements for
289 beam B3 (l_c = 25, 30, and 20 mm, respectively), and in the 4th, 5th and 9th elements for beam
290 B4 (l_c = 30, 15 and 20 mm, respectively).

By applying the crack parameters for each cracked beam specimen in the corresponding numerical model, the first five modes of natural frequencies and mode shapes of the beam specimens can be obtained.

For a comparison, the traditional reduced stiffness method as described in Eq. (9) earlier is also employed to model the effect of the cracks and predict the modal properties with the Timoshenko beam model. As a matter of fact, there is no simple way to match up an actual crack with an element stiffness reduction, for reasons as discussed in the "Overview of the cracked-beam element model and numerical verification" section. The same argument can be made even if a lumped rotational spring was involved, which could help address the discretization problem. Therefore, for a fairer comparison, herein the stiffness reduction is determined in an optimised manner. For beams with a single crack, there is just a single stiffness reduction (D) value on the element containing the crack; similarly for the beams with multiple cracks, multiple unknown D values are involved. The values of D are obtained by fitting the extracted and predicted modal data of the cracked beams through a model updating procedure. For this purpose the first five natural frequencies are used to form the objective function J_1 for the optimization problem concerning D, as:

$$J_1 = \frac{1}{5}\sum_{i=1}^{5} \mathrm{abs}\left(\frac{f_{\mathrm{dNm}i}^2}{f_{0\mathrm{Nm}i}^2} - \frac{f_{\mathrm{dNc}i}^2}{f_{0\mathrm{Nc}i}^2} \right) \tag{10}$$

where, $f_{\mathrm{N}i}$ represents the i^{th} natural frequency; subscripts 'c' and 'm' stand for computed and the extracted data, respectively; and subscripts 'd' and '0' stand for the damaged and intact states of the beam, respectively.

The selection of the optimal D value(s) is obtained through minimizing the above objective function using Genetic algorithm (GA). More details about the setting of GA will be given in the following section. The D values found from this process are subsequently employed in the reduced stiffness beam model to calculate the natural frequencies and mode

315 shapes. A comparison with the experimental results for each mode individually is then made
316 to examine the accuracy and consistency of the reduced stiffness model in representing the
317 cracks.

318 The verification is first carried out on the natural frequencies, and to simplify the
319 comparison a frequency shift indicator is introduced, which is defined as the relative change
320 of the i^{th} natural frequency of a cracked beam with respect to the intact state:

321 $$S_i = \frac{f_{0Ni} - f_{dNi}}{f_{0Ni}} \times 100\% \tag{11}$$

322 Thus for each cracked beam, the S_i values from the predicted natural frequencies using
323 the cracked beam element model and the reduced stiffness model, respectively, are compared
324 with S_i from the extracted results, as shown in Fig. 7. The predicted results using the cracked
325 beam element model match very well the experimental results for all the modes in all the four
326 cracked beams. The reduced stiffness model, on the other hand, achieves satisfactory
327 prediction only for the beam with a single shallow crack (B1). For beams with a deep crack
328 or multiple cracks, it cannot match all the modes. This confirms the observation mentioned in
329 'Overview of the cracked beam element model and numerical verification', and it further
330 indicates that different stiffness reduction factors would be needed to represent the effects of
331 the same crack on difference modes.

332 The Modal Assurance Criterion (MAC) values between the extracted and predicted mode
333 shapes of the cracked beams, which are defined in Eq. (12), are used to verify the accuracy of
334 the two models regarding mode shape calculation.

335 $$\mathrm{MAC}_i = \frac{\left(\phi_{dmi}^{T}\phi_{dci}\right)^2}{\left(\phi_{dmi}^{T}\phi_{dmi}\right)\left(\phi_{dci}^{T}\phi_{dci}\right)} \tag{12}$$

336 where, ϕ_i stands for the i^{th} mode shape vector of the beam; subscripts 'c' and 'm' stand for
337 computed and the extracted data, respectively.

Fig. 8 shows the comparison between the MAC values from the two different models. It can be seen that the MAC values from the cracked beam element model are all greater than 0.964 and exceed 0.990 for the first 3 modes, indicating very good match between the extracted and predicted mode shapes. However, the reduced stiffness model can only yield good MAC results for beam B1 with a single shallow crack. For the other beams, the MAC values are poor and this is particularly true for higher modes. In connection with the observations based on the natural frequencies in Fig. 7, it can be seen the accuracy in the predicted mode shapes using the reduced stiffness method tends to be poorer than the natural frequencies; the cracked beam element model, on the other hand, maintains consistent high accuracy for both.

Crack damage identification using the cracked beam element model

In this section the performance of the cracked beam element model when applied in crack damage identification is examined for the tested beam cases.

General consideration

The crack damage identification is carried out here using a finite element model updating procedure. For general applicability, each element in the FE model is considered as a potential cracked element and is modelled using the cracked beam element model with the crack depth ratio (α) and location (l_c) both unknown. Thus there is no limit on the number and locations of cracks to be identified in the beams. In the present situation, there are 12 elements in the beam model, so totally there are 24 unknown parameters. It is noted that the test beams under consideration had two free ends; as such the modal data (natural frequencies and mode shapes) would not be sensitive to the conditions in the elements at the beam ends. For simplicity and without losing generality, the two end elements in each beam are excluded from the updating operation and they are assumed to remain intact. This leaves 20 unknown

parameters to be determined (updated).

The objective function of the model updating is formed with the eigenvalue and mode shapes of the first five modes, as shown in Eq. (13),

$$J_2 = \frac{1}{N_{\mathrm{N}}}\sum_{i=1}^{N_{\mathrm{N}}} W_{fi}\cdot \mathrm{abs}\left(\frac{f_{\mathrm{dNm}i}^2}{f_{0\mathrm{Nm}i}^2}-\frac{f_{\mathrm{dNc}i}^2}{f_{0\mathrm{Nc}i}^2}\right)+\frac{1}{N_{\mathrm{S}}N_{\mathrm{n}}}\sum_{i=1}^{N_{\mathrm{S}}} W_{si}\cdot\left(\sum_{j=1}^{N_{\mathrm{n}}}\mathrm{abs}\left(\varphi_{\mathrm{m}ji}^{\mathrm{d}}-\varphi_{\mathrm{c}ji}^{\mathrm{d}}\right)\right) \qquad (13)$$

where, J_2 is the objective function to be minimised, N_{N} (= 5) is the number of natural frequencies to be included and N_{S} (= 5) is the number of mode shapes to be included. N_{n} (= 11) is the number of nodes in the extracted mode shapes. W_{fi} and W_{si} are the weights for the i^{th} eigenvalue and mode shape, respectively. The weights are generally chosen on the basis of the presumed measurement accuracy of the respective type of the modal data and are assigned to be unity here for simplicity.

Genetic algorithm (GA) is employed to search the optimization solution for the objective function J_2. GA is a global searching engine and has been widely used in finite element model updatings (Perera and Torres, 2006; Tu and Lu, 2008). Using a GA-based model updating eliminates the need to calculate the sensitivity matrix of the structure during the updating. Furthermore, the GA-based updating has no special requirement concerning the initial values of the updating parameters and has a higher probability of identifying a global optimum solution than the conventional gradient-based approach (Perera and Torres, 2006; Marwala, 2010). The GA function in Matlab is used in conjunction with the beam model to carry out the updatings.

Model updating results with a standard mesh setting

Model updating is first carried out with the above-mentioned standard beam model setting with 12 beam elements. The results are shown in Fig. 9 and Table 3.

Comparing with the actual crack conditions shown in Fig. 3 and summarised in Table 1, it can be seen that all the cracked elements have been identified correctly, with both the crack

386 depth and crack location being determined at good accuracy. For the beams with a single
387 crack (B1 and B2), the errors in the updated depth ratios (α) are smaller than 3%. For the
388 beams with multiple cracks (B3 and B4), the errors in the updated depth ratios are generally
389 smaller than 10%, except for the second crack in B4 which has an error of 23% and this is
390 explicable by the fact that it is a relatively shallow crack. It should also be noted that a false
391 crack is identified in the 11^{th} element in all of the beams. As has been explained in the
392 'General consideration' sub-section, this is attributable to the low sensitivity of the modal
393 data to changes in the elements close to the free end. The updated crack locations also have
394 very good accuracy. By defining a crack location error as the normalised difference in the
395 actual and updated crack positions within the element with respect to the element length, it
396 can be seen that the errors in the updated crack locations are generally lower than 10%. For
397 the beams with multiple cracks, all the cracked elements are identified clearly. It can
398 therefore be reasonably concluded that the crack damage identification with the cracked beam
399 model is effective for the thick beams with practically any combinations of cracks.

400 ***Crack damage identification with less modal information and coarser mesh setting***

401 In the last sub-section the updating was conducted by employing the lowest 5 modes of
402 modal data as input. However, for thick beams in a real life environment, measuring the first
403 5 modes, especially the mode shapes, to high accuracy could be difficult. Bearing this in
404 mind, an evaluation with reduced availability of the modal data, which usually necessitates a
405 reduced number of unknown parameters, is meaningful.

406 At this juncture, it is worth noting the fact that the present cracked beam element model
407 describes a crack in explicit terms, i.e., with explicit crack depth and crack location
408 parameters. Therefore in principle the model allows the use of a reduced number of elements
409 for the beam without a gross loss of precision as would be the case when a reduced stiffness
410 method is used. It should be noted here that by 'precision' it does not mean one will not get a

411 converged solution with equivalent measures such as the reduced stiffness; however, without
412 an explicit description of the crack such a solution will become less meaningful as it will tend
413 to dilute the locality of the damage with less number of elements. This problem is effectively
414 removed with the use of the cracked element model.

415 Herein the performance of cracked element model for updating with a reduced amount of
416 extracted modal information is examined. Only the lowest three modes of eigenvalues and
417 mode shapes are considered, and the same objective function as shown in Eq. (13) is used. In
418 correspondence with the reduced amount of input information, a coarser mesh with a uniform
419 element length (l_e) equal to 100 mm is used in the beam model, making the total number of
420 elements to be 6. After excluding the two elements at the free ends, there are 8 parameters to
421 be updated in the beam model.

422 The results for the crack damage identification using the above modal data and mesh
423 setting are shown in Fig. 10 and Table 4. Note that with the current mesh setting, for beams
424 B1 and B2 the correct cracked element should be the 4th element with l_c = 75 mm; for beam
425 B3 and B4 the cracked elements should be the 2nd, 3rd and 5th elements with l_c = 25, 30 and 20
426 mm and 80, 15, 20 mm, respectively. It can be seen that very accurate updating results can
427 still be obtained. All the cracked elements are identified correctly, and errors in the updated
428 crack depth ratios are less than 2% for the single-crack beams and generally lower than 10%
429 for the multiple-crack beams. The errors in updated crack locations are lower than 15% for all
430 the beams.

431 The above outcome with a reduced order of modal data being employed in conjunction
432 with a coarse discretization is very favourable for practical applications, and apparently this
433 characteristic is unique with the current cracked element model because of the explicit
434 description of the crack parameters.

435 It should be noted, however, that the present cracked beam element model assumes just

436 one crack within an individual element length. With a coarse mesh setting and a larger
437 element size, there will be increased likelihood that more than one crack may actually occur
438 within an element length. One way to deal with such a scenario is to conduct several parallel
439 updatings with different schemes of discretisation. By inspecting and comparing the results,
440 one should be able to assess if multiple cracks might exist within a limited length of the beam.
441 On this basis, partially refined discretisation with variable element lengths may be considered
442 to finally identify the crack parameters.

443 **Crack damage identification with artificial boundary condition (ABC) frequencies**

444 In vibration-based model updating practice, natural frequencies and mode shapes are the
445 most widely used modal parameters, and these data have been employed in the updating
446 cases in the last section. Considering the fact that in real life applications mode shape data are
447 often difficult to measure to satisfactory accuracy (Jones and Turcotte, 2002; Mottershead
448 and Friswell, 1993), a lot of efforts have been devoted to find alternative modal parameters
449 for structural model updating. One approach is using the so-called artificial boundary
450 condition frequencies, or in short ABC frequencies as mentioned earlier. In this section, the
451 effectiveness of incorporating the ABC frequencies for the crack identification using the
452 cracked element model is examined on the test beams. For the sake of completeness, a brief
453 introduction of the ABC frequencies is presented.

454 ***Brief overview of the ABC frequencies***

455 The concept of ABC frequencies (Gordis, 1996; 1999) can be better understood by its
456 analogy to the perturbed boundary condition technique. In the perturbed boundary condition
457 method, new modal information is generated by physically altering the boundary conditions
458 of the tested structures; thus additional modal frequencies are made available for the same
459 structure under different boundary conditions (Li, et al., 1995). However, it is impractical to

actually change the boundary conditions of a real structure due to the costs and technical difficulties. The ABC frequency technique, on the other hand, is devised in attempt to obtain the natural frequencies of a structure with perturbed boundary conditions but without the need to physically alter the structure. Gordis (1996, 1999) has shown that these frequencies can be established by manipulating the incomplete frequency response function (FRF) matrix extracted from the existing structure. This also explains the term 'artificial boundary condition'.

The idea of acquiring the ABC frequencies can be illustrated schematically in Fig. 11 (a). Suppose the natural frequencies of the structure with two additional pins at point *i* and *j* are to be obtained. Instead of physically adding these pins, conventional modal tests are carried out on the original structure at points *i* and *j* as shown in Fig. 11 (b). By exciting the structure at point *i* and *j* separately, four FRF curves, namely FRF_{ii}, FRF_{ij}, FRF_{ji} and FRF_{jj} can be obtained. These four ABC curves can then be used to form the incomplete FRF matrix $\mathbf{H}_{mm}$, as:

$$\mathbf{H}_{mm} = \begin{bmatrix} FRF_{ii} & FRF_{ij} \\ FRF_{ji} & FRF_{jj} \end{bmatrix} \tag{14}$$

It can be proven that the natural frequencies of the intended structure with two additional pins, shown in Fig. 11(a), are equal to the resonance frequencies of the elements in the inverted $\mathbf{H}_{mm}$ (i.e. $\mathbf{H}_{mm}^{-1}$), providing the structure is undamped or lightly-damped. Using the ABC terminology, these are two-pin ABC frequencies.

Apparently, for one-pin scenarios, the ABC frequencies degenerate to the antiresonances of the driving FRF. For example, the one-pin ABC frequencies with 'pin' at point *i* are the antiresonances of FRF_{ii}. In fact, one-pin ABC frequencies (antiresonances) have been widely used in the model updating on laboratory experimental structures, including frames, trusses and beams (D'Ambrogio and Fregolent, 2000; Dilena and Morassi, 2010; Jones and Turcotte,

2002). Results suggest that one-pin ABC frequencies can effect to enhance the model updating of experimental structures. Two-pin ABC frequencies have not been extensively applied in model updating practice. Tu and Lu (2008) used numerically simulated structures to demonstrate the effectiveness of one-pin and two-pin ABC frequencies for the model updating of several frame structures.

Obtaining ABC frequencies from the test beams

To generate sufficient ABC frequencies, some supplementary tests were carried out on the beams described in the 'Test specimens' sub-section. Driving excitations were applied on points P0, P2, P4, P8, P10, and P12 separately to facilitate the extraction of the one-pin ABC frequencies at these points. To generate the two-pin ABC curves at point (i, j), two accelerometers were attached at point i and j and excitations were carried out at the two points successively. Referring to Fig. 4(b), the following two-pin configurations were tested: (i, j) = (P0, P12), (P0, P6), (P6, P12), (P2, P8) and (P4, P10).

The same signal processing strategy presented in the 'Modal testing setup' sub-section was used to obtain the FRF curves as well as ABC curves. However, it should be pointed out that extracting ABC frequencies poses higher demand on the quality of the FRF curves as compared with natural frequencies. As the one-pin ABC frequencies are extracted from the antiresonances of FRF curves and the two-pin ABC frequencies are generally away from the resonances of FRF curves, the signal to noise ratio (SNR) in the vicinity of ABC frequencies is generally lower than that of natural frequencies. To tackle this problem, the multi-DOF modal analysis method Rational Fraction Polynomial (RFP) method (Richardson and Formenti, 1982) is employed to smooth the extracted FRF and ABC curves and extract the ABC frequencies. Representative FRF curve and ABC curves before and after applying RFP are shown in Fig. 12. It can be seen that it is straightforward to find the ABC frequencies from the RFP-processed curves.

The lowest 3 modes of one-pin and two-pin ABC frequencies (denoted as f_A) from the above configurations were extracted from the FRF and ABC curves. Selected results are presented in Table 5 and 6. It shows that the shifts of ABC frequencies brought by the cracks are around the similar range as that of natural frequencies.

FE model updating with ABC frequencies

The obtained one-pin and two-pin ABC frequencies are then used to perform model updating on the cracked beams. Two new objective functions with combined natural frequencies and one-pin ABC frequencies (J_3) or two-pin ABC frequencies (J_4) are used in the updatings, as:

$$J_3 = \frac{1}{N_N}\sum_{i=1}^{N_N} W_i \cdot \mathrm{abs}\left(\frac{f_{dNmi}^2}{f_{0Nmi}^2} - \frac{f_{dNci}^2}{f_{0Nci}^2}\right) + R_0 + R_2 + R_4 + R_8 + R_{10} + R_{12} \quad (15)$$

$$J_4 = \frac{1}{N_N}\sum_{i=1}^{N_N} W_i \cdot \mathrm{abs}\left(\frac{f_{dNmi}^2}{f_{0Nmi}^2} - \frac{f_{dNci}^2}{f_{0Nci}^2}\right) + R_{0,12} + R_{0,6} + R_{6,12} + R_{2,8} + R_{4,10} \quad (16)$$

In the equations, R is a residual from the extracted and computed one-pin or two-pin ABC frequencies, as expressed in Eq. (17). The subscript number of R indicates the 'pin' number. For example, R_2 is related to one-pin frequencies with 'pin' at point P2, and $R_{2,8}$ is related to two-pin ABC frequencies with 'pins' at points P2 and P8.

$$R = \frac{1}{N_A}\sum_{i=1}^{N_A} \mathrm{abs}\left(\frac{f_{dAmi}^2}{f_{0Ami}^2} - \frac{f_{dAci}^2}{f_{0Aci}^2}\right) \quad (17)$$

where, f_A stands for the one-pin or two-pin ABC frequencies. N_A is the modes of ABC frequencies used, which is set as 3 herein. Other symbols have the same meanings as in Eq. (13).

It should be noticed that while extracted ABC frequencies in Eq. (17) were obtained from the modal tests, their computed counterparts can be easily calculated by adding the additional pins in the FE model.

The coarse mesh setting with l_c = 100 mm is applied in the beam model. Fig. 13 shows the results in terms of the crack depth in each element from the model updating with a combined natural and one-pin ABC frequencies (Eq. 15). It can be seen that very good updating results are obtained with the inclusion of the ABC frequencies. All the cracked elements can be identified with errors in crack depth ratios (α) less than 3% for single-crack beams and generally less than 10% for multiple-crack beams (except the shallow crack in beam B4 with an error of 20%). A check of the updated relative positions of the cracks within the individual elements (not shown here) indicates that the crack positions are identified with a similar level of accuracy as mentioned above.

The crack depths from using a combination of the natural and two-pin ABC frequencies are shown in Fig. 14. The results are also satisfactory. It should be noted that the test beams were quite stiff and this rendered the two-pin ABC frequencies to be in a high frequency range, and thus generally increased measurement error, particularly in the two-pin ABC cases.

The incorporation of the ABC frequencies actually provides a scope to expand dramatically the modal frequency data set, and this is deemed to be very beneficial for updating with the cracked beam element model because of the generally increased demand on the updating. With an appropriate sensitivity analysis (Tu and Lu, 2008), it is possible to choose the most sensitive configurations of pin locations to generate enough ABC frequencies for updatings with a large number of unknown parameters.

Conclusions

An experimental study has been conducted to investigate the effectiveness of a cracked beam element model for the identification of crack damage in thick beams with extracted modal data. Laboratory beam specimens with a length to thickness ratio around 10 were prepared with different crack scenarios, and modal testing was performed on these beams to

555 extract the natural frequencies and mode shapes.

556 From the comparison between the extracted modal data and those predicted counterparts
557 using the cracked beam element model, it can be concluded that the cracked beam element
558 model is sufficiently accurate in both single- and multiple-crack beam scenarios, and the
559 accuracy is consistent across all modes being examined. In contrast, the conventional reduced
560 stiffness model cannot achieve consistent accuracy in representing the crack effect on the
561 extracted natural frequencies and mode shapes for different modes.

562 The performance of the cracked beam element model in an inverse process to identify the
563 crack parameters has been assessed with a finite element model updating procedure. Using
564 the extracted modal data from the tested beams, very good identification results have been
565 achieved. In fact all cracked elements can be found correctly; and in most cases the crack
566 depth and crack positions can be determined with high accuracy. It has also been
567 demonstrated that in cases where the available modal data may be limited (for example to the
568 lowest three modes), the cracked beam element model can still yield satisfactory crack
569 identification with a coarse element discretization.

570 The cracked beam element model exhibits equally satisfactory results when the extracted
571 modal data is comprised of the natural frequencies and the 'ABC' frequencies which replace
572 the mode shape data. In view of the fact that a variety of the ABC configurations exist, the
573 incorporation of the ABC frequencies opens up an additional scope for the application of the
574 cracked beam element model, especially in more complex situations where a large number of
575 crack parameters may need to be identified.

576 It should be noted that the cracked beam element model being investigated has been
577 formulated for a rectangular cross section. For other cross section types such as a box section,
578 the additional flexibility matrix will need to be re-formulated and subsequently verified with
579 experiments of similar cross section properties.

Another point to be noted is that the verification and demonstration in the present experimental study has been designed to focus on the so-called 'model' error concerning cracks, and with the cracked beam element model such error is effectively reduced and this can be achieved in a physical test. However, in a real structural environment such as beams being parts of a larger structure, many other complexities may be involved, and these need to be addressed in conjunction with enhancement of the basic modelling approach.

Acknowledgements

The research reported in the paper is partly funded by the Chinese Scholarship Council and the University of Edinburgh through a joint scholarship for the PhD study of the first author.

References

Cabib, E., Freddi, L., Morassi, A., and Percivale, D. (2001). "Thin notched beams." *J. Elasticity*, 64(2), 157-178.

Caddemi, S., and Morassi, A. (2013). "Multi-cracked Euler-Bernoulli beams: mathematical modelling and exact solutions." *Int. J.Solids Struct.*, 50(6), 944-956.

Chondros, T. G., Dimarogonas, A. D., and Yao, J. (1998). "A continuous cracked beam vibration theory." *J. Sound Vib.*, 215(1), 17-34.

Christides, S., and Barr, A. D. S. (1984). "One-dimensional theory of cracked Bernoulli-Euler beams." *Int. J. Mech. Sci.*, 26(11-1), 639-648.

D'Ambrogio, W., and Fregolent, A. (2000). "The use of antiresonances for robust model updating." *J. Sound Vib.*, 236(2), 227-243.

Dilena, M., and Morassi, A. (2010). "Reconstruction method for damage detection in beams based on natural frequency and antiresonant frequency measurements." *J. Eng. Mech.*, 10.1061/(ASCE)0733-9399(2010)136:3(329), 329-344.

Dimarogonas, A. D., and Papadopoulos, C. A. (1983). "Vibration of cracked shafts in bending." *J. Sound Vib.*, 91(4), 583-593.

Friswell, M. I., and Penny, J. E. T. (2002). "Crack modeling for structural health monitoring." *Struct. Health Monit.*, 1(2), 139-148.

Gordis, J. H. (1999). "Artificial boundary conditions for model updating and damage detection." *Mech. Syst. Signal Pr.*, 13(3), 437-448.

Gordis, J. H. (1996). "Omitted coordinate systems and artificial constraints in spatially incomplete identification." *Modal Anal.*, 11(1-2), 83-95.

Jones, K., and Turcotte, J. (2002). "Finite element model updating using antiresonant frequencies." *J. Sound Vib.*, 252(4), 717-727.

Lee, Y. S., and Chung, M. J. (2000). "A study on crack detection using eigenfrequency test data." *Comput. Struct.*, 77(3), 327-342.

Li, S. M., Shelley, S., and Brown, D. (1995). "Perturbed boundary condition testing concepts. " *Proc., 13th Int. Modal Anal. Conf.*, Society of Experimental Mechanics, Inc., Nashville, Tennessee, 902-907.

Marwala, T. (2010). *Finite element model updating using computational intelligence techniques: applications to structural dynamics*, Springer.

Morassi, A. (2001). "Identification of a crack in a rod based on changes in a pair of natural frequencies." *J. Sound Vib.*, 242(4), 577-596.

Mottershead, J. E., and Friswell, M. I. (1993). "Model updating in structural dynamics - A survey." *J. Sound Vib.*, 167(2), 347-375.

Narkis, Y. (1994). "Identification of crack location in vibrating simply supported beams." *J. Sound Vib.*, 172(4), 549-558.

Papadopoulos, C. A., and Dimarogonas, A. D. (1987a). "Coupled longitudinal and bending vibrations of a rotating shaft with an open crack." *J. Sound Vib.*, 117(1), 81-93.

629 Papadopoulos, C. A., and Dimarogonas, A. D. (1987b). "Coupling of bending and torsional
630 vibration of a cracked Timoshenko shaft." *Ing. Arch.*, 57(4), 257-266.
631 Perera, R., and Torres, R. (2006). "Structural damage detection via modal data with Genetic
632 Algorithms." *J. Struct. Eng.*, 10.1061/(ASCE)0733-9445(2006)132:9(1491), 1491-1501.
633 Richardson, M. H., and Formenti, D. L. (1982). "Parameter estimation from frequency
634 response measurements using Rational Fraction Polynomials." *Proc., 1st Int. Modal Anal.*
635 *Conf.*, Society of Experimental Mechanics, Inc., Orlando, Florida, 167-186.
636 Rubio, L., Fernandez-Saez, J., and Morassi, A. (2015a). "Crack identification in non-uniform
637 rods by two frequency data." *Int. J.Solids Struct.*, 75-76(1), 61-80.
638 Rubio, L., Fernandez-Saez, J., and Morassi, A. (2015b). "Identification of two cracks in a rod
639 by minimal resonant and antiresonant frequency data." *Mech. Syst. Signal Pr.*, 60-61, 1-
640 13.
641 Ruotolo, R., and Surace, C. (1997). "Damage assessment of multiple cracked beams:
642 Numerical results and experimental validation." *J. Sound Vib.*, 206(4), 567-588.
643 Sinha, J. K., Friswell, M. I., and Edwards, S. (2002). "Simplified models for the location of
644 cracks in beam structures using measured vibration data." *J. Sound Vib.*, 251(1), 13-38.
645 Swamidas, A. S. J., Yang, X., and Seshadri, R. (2004). "Identification of cracking in beam
646 structures using Timoshenko and Euler formulations." *J. Eng. Mech.*,
647 10.1061/(ASCE)0733-9399(2004)130:11(1297), 1297-1308.
648 Tada, H., Paris, P. C., and Irwin, G. R. (2000). *The stress analysis of cracks handbook*,
649 ASME Press, New York, US.
650 Tu, Z. G., and Lu, Y. (2008). "FE model updating using artificial boundary conditions with
651 Genetic Algorithms." *Comput. Struct.*, 86(7-8), 714-727.
652

Figure Captions

Fig. 1. Loading state of a cracked beam element

Fig. 2. A comparison between predicted and numerically simulated natural frequencies for cracked beam: (a) Cracked beam being analysed (Unit: mm); (b) Comparison for the first 6 natural frequencies

Fig. 3. Beam specimens and configurations of cracks

Fig. 4. Modal testing setup: (a) Photo of test setup; (b) Schematic view of the setup and measurement arrangement (Unit: mm)

Fig. 5. A typical extracted FRF curve from measurement

Fig. 6. Extracted mode shapes from all 5 beam specimens: (a) 1st mode; (b) 2nd mode

Fig. 7. Comparison between frequency shifts: (a) B1; (b) B2; (c) B3; (d) B4

Fig. 8. Comparison between MAC results: (a) B1; (b) B2; (c) B3; (d) B4

Fig. 9. Updated crack depth ratios (α) with standard mesh setting: (a) B1; (b) B2; (c) B3; (d) B4

Fig. 10. Updated crack depth ratios (α) with coarser mesh setting: (a) B1; (b) B2; (c) B3; (d) B4

Fig. 11. Illustration of artificial boundary condition frequency measurement settings: (a) Simply supported beam with a 'perturbed' boundary condition with added pins at '*i*' and '*j*'; (b) Artificial boundary condition frequency measurements

Fig. 12. RFP technique for noisy antiresonances and two-pin ABC frequencies: (a) FRF curve (close-in); (b) Two-pin ABC curve (close-in)

Fig. 13. Updated crack depth ratios (α) with J_3: (a) B1; (b) B2; (c) B3; (d) B4

Fig. 14. Updated crack depth ratios (α) with J_4: (a) B1; (b) B2; (c) B3; (d) B4

Tables

Table 1. Crack information of the aluminium beam specimens

Beam label	Crack1		Crack2		Crack3	
	α	L_c/mm	α	L_c/mm	α	L_c/mm
B0	-	-	-	-	-	-
B1	0.3	375	-	-	-	-
B2	0.5	375	-	-	-	-
B3	0.35	125	0.25	230	0.4	420
B4	0.35	180	0.25	215	0.4	420

Table 2. Extracted natural frequencies f_N (±% denotes relative change from B0)

Mode	B0 (Hz)	B1		B2		B3		B4	
		(Hz)	±%	(Hz)	±%	(Hz)	±%	(Hz)	±%
1	725.1	673.8	**7.1**	577.7	**20.3**	629.1	**13.2**	609.9	**15.9**
2	1912.6	1825.1	**4.6**	1702.3	**11.0**	1533.1	**19.8**	1481.7	**22.5**
3	3547.3	3532.9	**0.4**	3493.4	**1.5**	3022.8	**14.8**	3228.7	**9.0**
4	5493.9	5269.7	**4.1**	5142.4	**6.4**	5051.1	**8.1**	5273.6	**4.0**
5	7673.6	7560.6	**1.5**	7422.6	**3.3**	6894.3	**10.2**	7010.4	**8.6**

Table 3. Updated crack locations (l_c) with standard mesh setting

Element number	1	2	3	4	5	6	7	8	9	10	11	12
B1	-	-	-	-	-	-	-	25.6	-	-	-	-
B2	-	-	-	-	-	-	-	24.9	-	-	-	-
B3	-	-	27.1	-	35.6	-	-	-	24.9	-	-	-
B4	-	-	-	32.2	17.4	-	-	-	23.7	-	-	-

Table 4. Updated crack locations (l_c) with coarser mesh setting

Element number	1	2	3	4	5	6
B1	-	-	-	74.3	-	-
B2	-	-	-	76.2	-	-
B3	-	23.3	28.1	-	31.1	-
B4	-	96.8	18.7	-	32.6	-

Table 5. One-pin ABC frequencies with 'pin' at P4 (f_A)

Mode	B0	B1		B2		B3		B4	
	(Hz)	(Hz)	±%	(Hz)	±%	(Hz)	±%	(Hz)	±%
1	594.2	565.8	**4.8**	508.8	**14.4**	517.6	**12.9**	476.7	**19.8**
2	1387.4	1284.8	**7.4**	1140.1	**17.8**	1139.7	**17.9**	1079.6	**22.2**
3	3466.7	3466.6	**0.0**	3440.4	**0.8**	3015.3	**13.0**	3125.4	**9.8**

Table 6. Two-pin ABC frequencies with 'pins' at P4 and P10 (f_A)

Mode	B0	B1		B2		B3		B4	
	(Hz)	(Hz)	±%	(Hz)	±%	(Hz)	±%	(Hz)	±%
1	562.3	533.6	**5.1**	479.1	**14.8**	489.3	**13.0**	452.4	**19.5**
2	1378.2	1277.4	**7.3**	1137.4	**17.5**	1130.8	**18.0**	1076.0	**21.9**
3	2652.8	2675.2	**-0.8**	2596.3	**2.1**	2570.5	**3.1**	2465.0	**7.1**

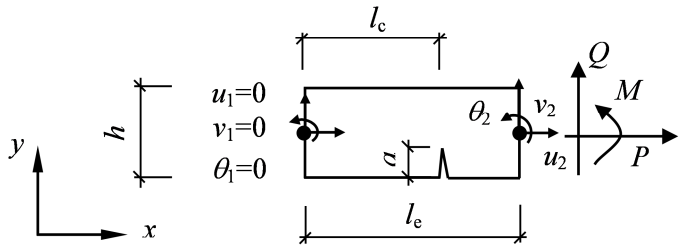

Fig. 1. Loading state of a cracked beam element

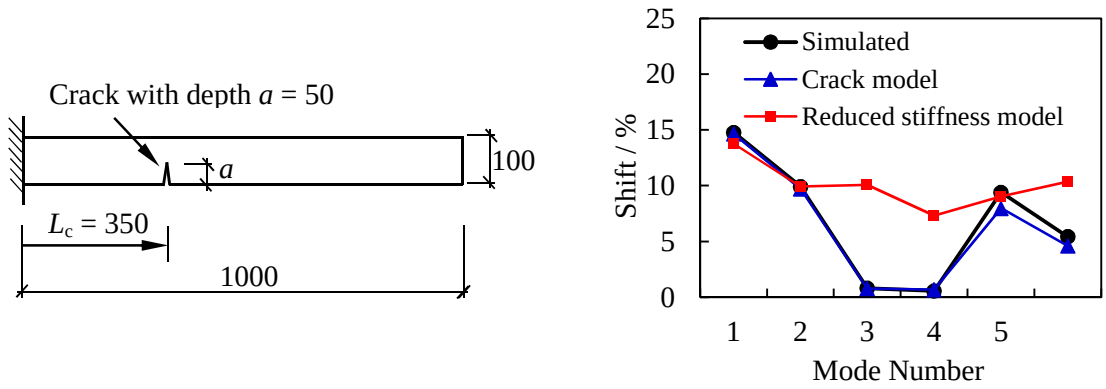

(a) (b)

Fig. 2. A comparison between predicted and numerically simulated natural frequencies for cracked beam: (a) Cracked beam being analysed (Unit: mm); (b) Comparison for the first 6 natural frequencies

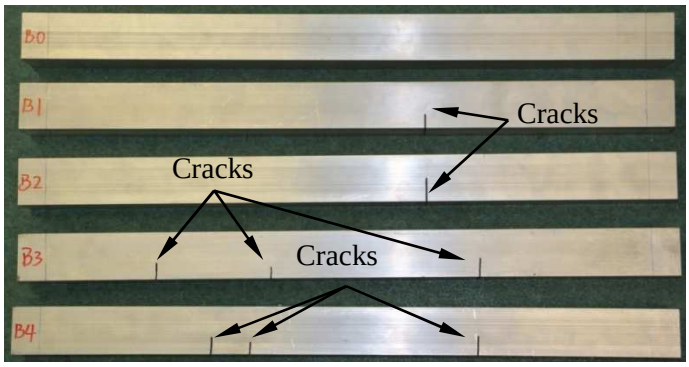

Fig. 3. Beam specimens and configurations of cracks

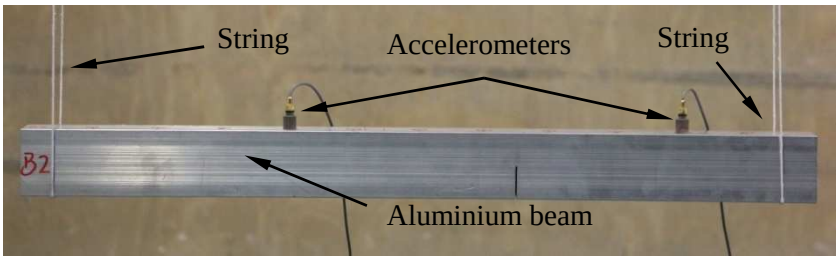

(a)

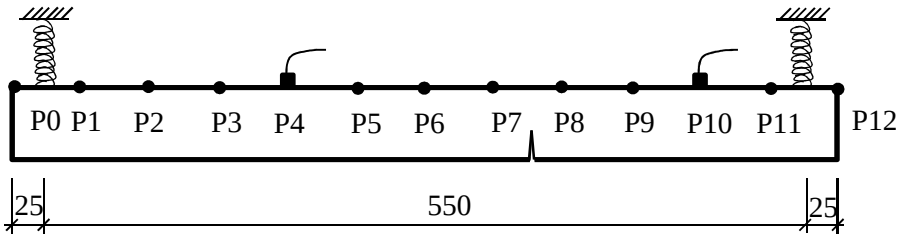

(b)

Fig. 4. Modal testing setup: (a) Photo of test setup; (b) Schematic view of the setup and measurement arrangement (Unit: mm)

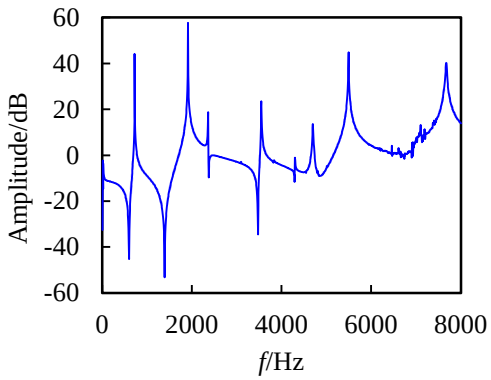

Fig. 5. A typical extracted FRF curve from measurement

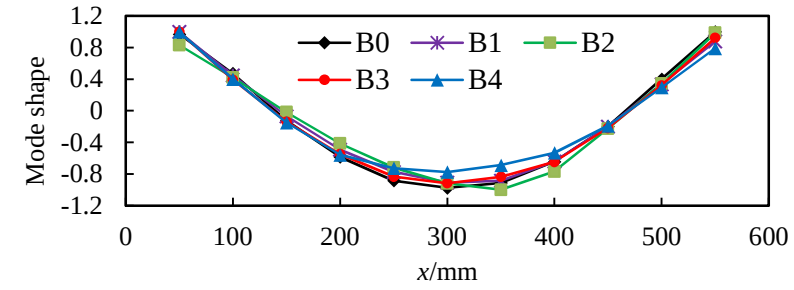

(a)

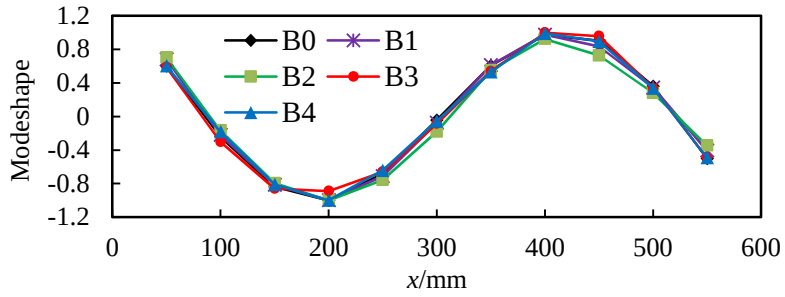

(b)

Fig. 6. Extracted mode shapes from all 5 beam specimens: (a) 1st mode; (b) 2nd mode

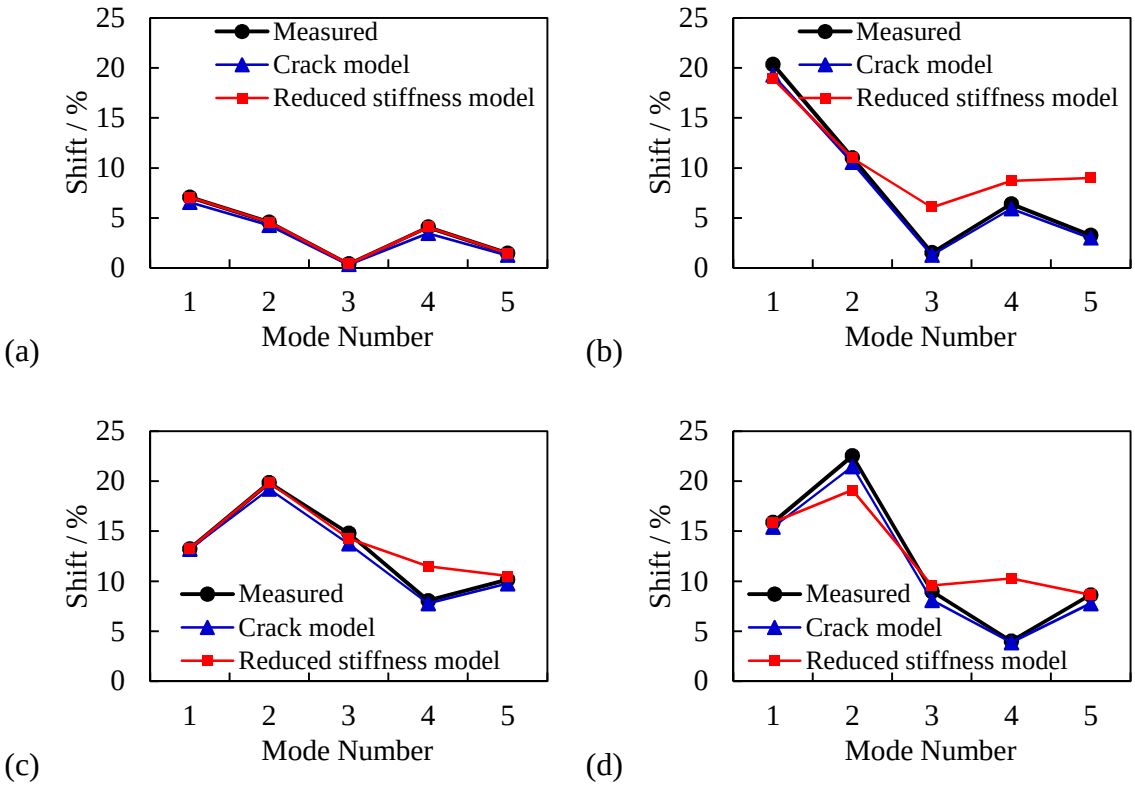

Fig. 7. Comparison between frequency shifts: (a) B1; (b) B2; (c) B3; (d) B4

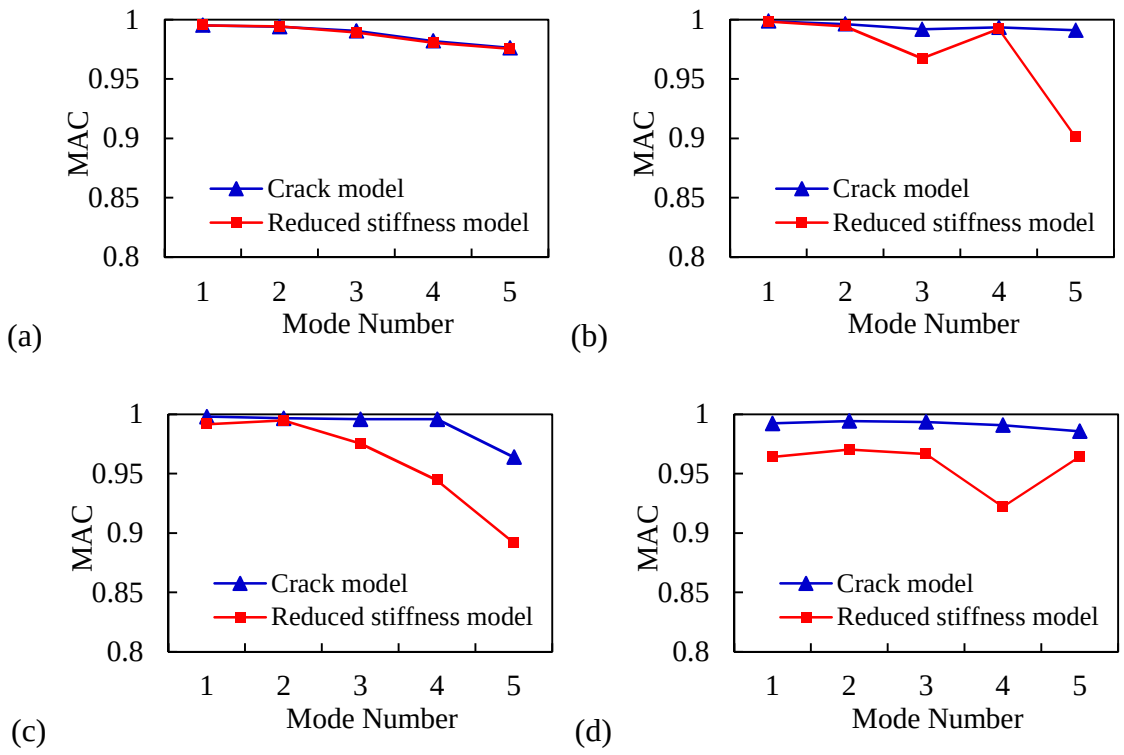

Fig. 8. Comparison between MAC results: (a) B1; (b) B2; (c) B3; (d) B4

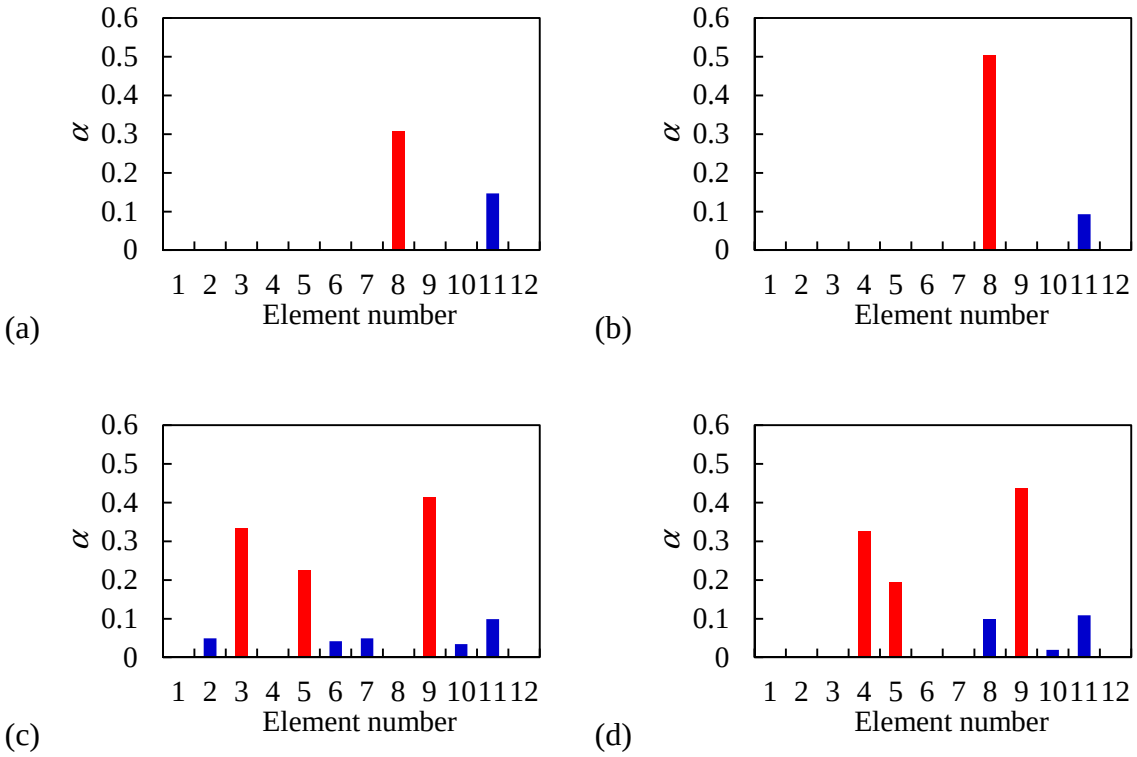

Fig. 9. Updated crack depth ratios (α) with standard mesh setting: (a) B1; (b) B2; (c) B3; (d) B4

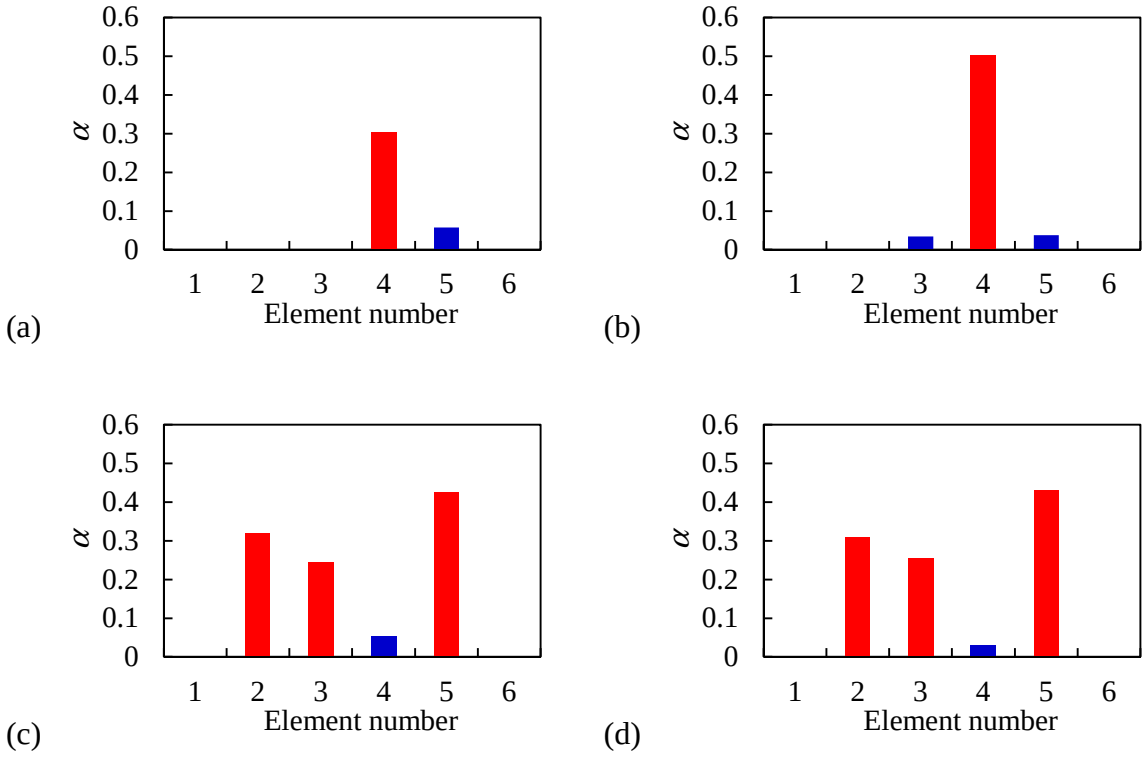

Fig. 10. Updated crack depth ratios (α) with coarser mesh setting: (a) B1; (b) B2; (c) B3; (d) B4

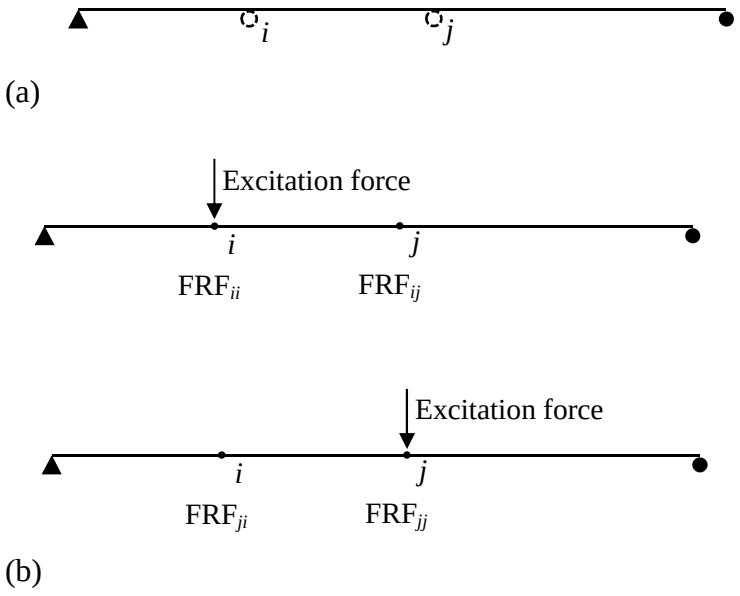

Fig. 11. Illustration of artificial boundary condition frequency measurement settings: (a) Simply supported beam with a 'perturbed' boundary condition with added pins at '*i*' and '*j*'; (b) Artificial boundary condition frequency measurements

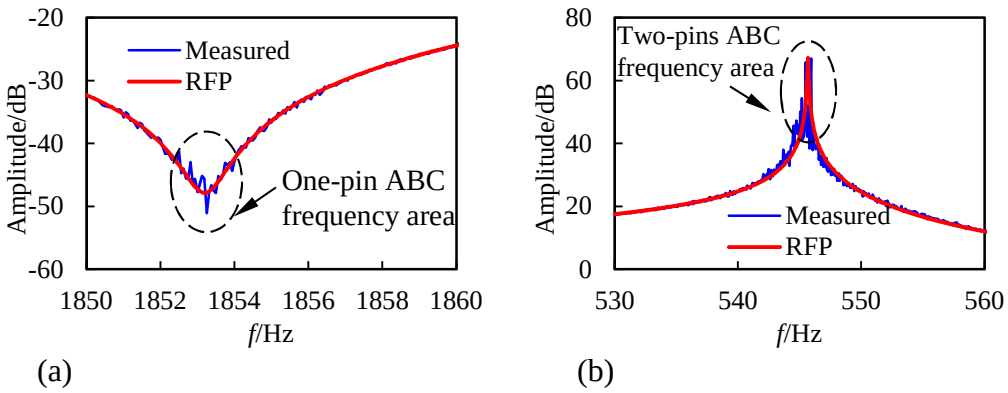

Fig. 12. RFP technique for noisy antiresonances and two-pin ABC frequencies: (a) FRF curve (close-in); (b) Two-pin ABC curve (close-in)

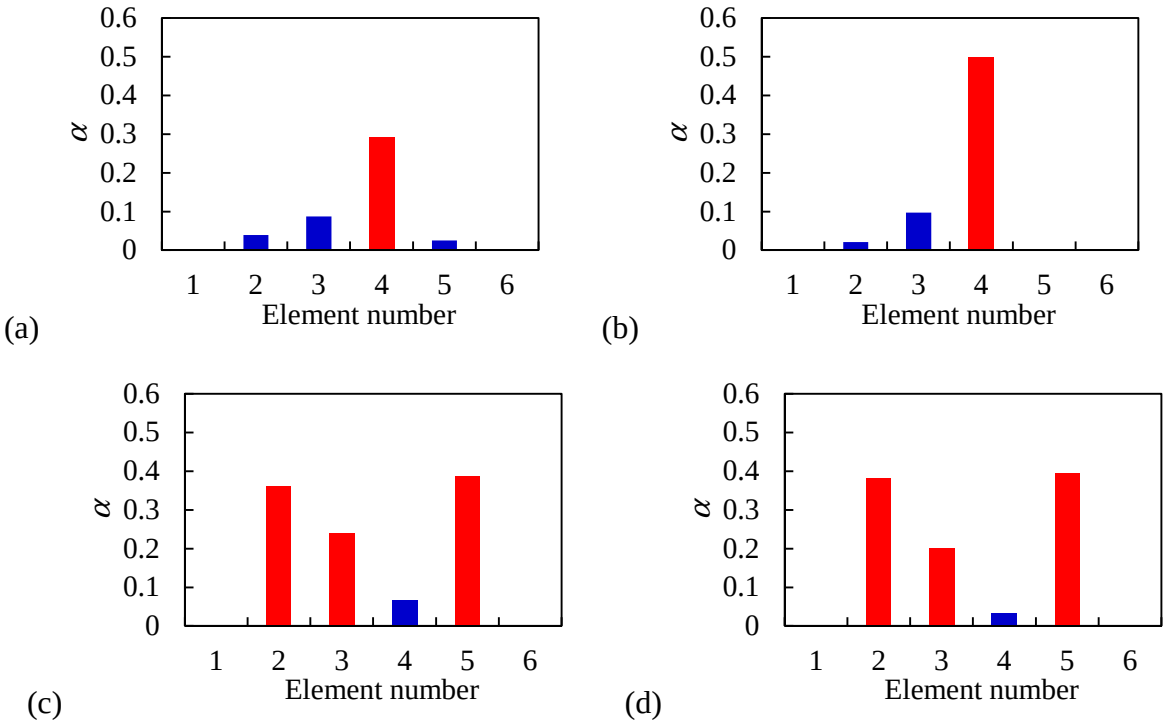

Fig. 13. Updated crack depth ratios (α) with J_3: (a) B1; (b) B2; (c) B3; (d) B4

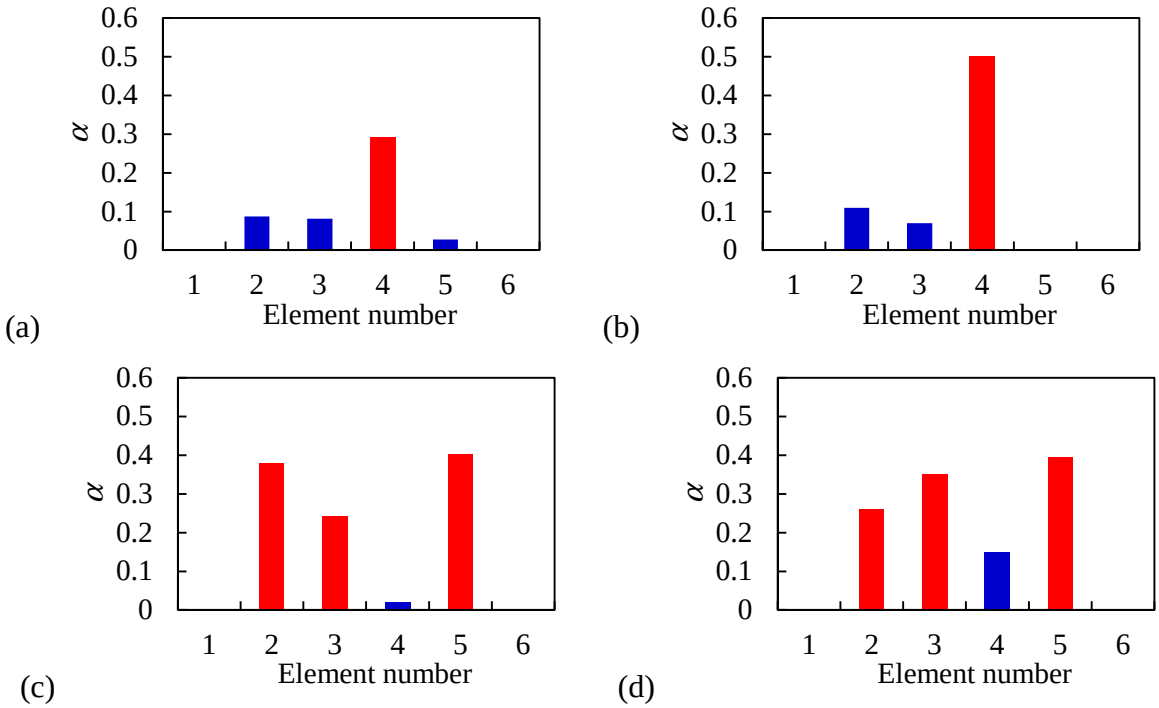

Fig. 14. Updated crack depth ratios (α) with J_4: (a) B1; (b) B2; (c) B3; (d) B4